Journal of Power Sources 195 (2010) 2669–2676

Contents lists available at ScienceDirect

Journal of Power Sources

journal homepage: www.elsevier.com/locate/jpowsour

Wet-etching of precipitation-based thin film microstructures for micro-solid oxide fuel cells

Jennifer L.M. Rupp*, Ulrich P. Muecke, Prathima C. Nalam, Ludwig J. Gauckler

Department of Materials, ETH Zurich, ETH Zurich Wolfgang-Pauli-Str. 10, CH-8093 Zurich, Switzerland

ARTICLE INFO

Article history:
Received 24 August 2009
Accepted 19 November 2009
Available online 26 November 2009

Keywords:
Micro-solid oxide fuel cells
Portable electronics
Thin films
Etching
Ceria
Microfabrication

ABSTRACT

In micro-solid oxide fuel cells (μ-SOFCs) ceramic thin films are integrated as free-standing membranes on micromachinable substrates such as silicon or Foturan® glass ceramic wafers. The processing of μ-SOFCs involves unavoidable dry- or wet-chemical etching for opening the substrate below the free-standing fuel cell membranes. In the first part of this paper current dry- and wet-chemical etchants for structuring of ceria-based electrolyte materials are reviewed, and compared to the etch-rates of common μ-SOFCs substrates. Wet-chemical etchants such as hydrofluoric acid are of high interest in μ-SOFC processing since they allow for homogeneous etching of ceria-based electrolyte thin films contrary to common dry-etching methods. In addition, HF acid is the only choice for substrate etching of μ-SOFC based on Foturan® glass ceramic wafers. Etching of $Ce_{0.8}Gd_{0.2}O_{1.9-x}$ spray pyrolysis electrolyte thin films with 10% $HF:H_2O$ is investigated. The etch-resistance and microstructures of these films show a strong dependency on post deposition annealing, i.e. degree of crystallinity, and damage for low acid exposure times. Their ability to act as a potential etch-resistance for μ-SOFC membranes is broadly discussed. Guidance for thermal annealing and etching of $Ce_{0.8}Gd_{0.2}O_{1.9-x}$ thin films for the fabrication of Foturan®-based μ-SOFCs is given.

© 2009 Elsevier B.V. All rights reserved.

1. Microfabrication of micro-solid oxide fuel cells devices

Micro-solid oxide fuel cells (μ-SOFCs) are potentially an alternative power supply to Li-ion batteries for portable electronics operating on fuel and air, independent from the electric net [1–3]. The first proof-of-concept for power delivery of these membranes was illustrated recently for low operating temperatures between 100 and 600 °C [4–6]. This new type of solid oxide fuel cell requires the active cell components as tri-layers of cathode electrolyte and anode thin films forming a mechanically free-standing fuel cell membrane integrated on a substrate. A schematic view of a state-of-the-art μ-SOFC membrane is displayed in Fig. 1. The active electrochemical cells of μ-SOFCs are made by free-etching of the substrate underneath the fuel cell membrane to allow for the gas access on both sides. Depending on the choice of substrate for the μ-SOFC, i.e. silicon [4] or Foturan® glass–ceramic-based wafers [5] dry- or wet-chemical etchants are used, accordingly.

Foturan® glass–ceramic wafer substrates are advantageous compaired to Si-based ones for fabrication, as they are electrical insulators. Therefore, no additional SiO_2 or Si_3N_4 insulating coatings are needed in contrast to Si-wafer-based μ-SOFCs [7–9]. Thermal expansion coefficients close to the ceramic μ-SOFC thin film layers [10] and the possibility to structure via selective UV-exposure through shadow masks without the use of conventional photoresists [7] are attractive. However, the only suitable etchant for structuring of Foturan® glass–ceramic-based wafers is etching with a solution of 10% $HF:H_2O$ acid [7,10]. Microstructering of μ-SOFC membranes on base of Foturan® glass–ceramic wafers remains challenging as HF acid is known to be very aggressive and its reaction on the fuel cell thin film microstructures, as well as their etch-rates are almost nonexistent. In conclusion, this leads to low yields in device microfabrication, as the etch processes are difficult to control. A typical Foturan®-based μ-SOFC membrane [5,11,12] as well as one of its electrolytes formed by the precipitation-based method of spray pyrolysis from $Ce_{0.8}Gd_{0.2}O_{1.9-x}$ is presented [13,14] (Fig. 2). Due to the given advantages of μ-SOFC processing based on Foturan® glass–ceramic-based wafers we concentrate in this paper on structuring of $Ce_{0.8}Gd_{0.2}O_{1.9-x}$ thin films by 10% $HF:H_2O$ etching, and the impact of the initial film microstructure on its etch-resistance. In order to compare and value achieved etch-rates and microstructures we review in the following current dry- and wet-chemical etchants and etch-rates for structuring of ceria-based thin films always in view of the common μ-SOFC substrate materials.

* Corresponding author. Tel.: +41 44 632 5651; fax: +41 44 632 1132.
E-mail address: jennifer.rupp@mat.ethz.ch (J.L.M. Rupp).

0378-7753/$ – see front matter © 2009 Elsevier B.V. All rights reserved.
doi:10.1016/j.jpowsour.2009.11.082

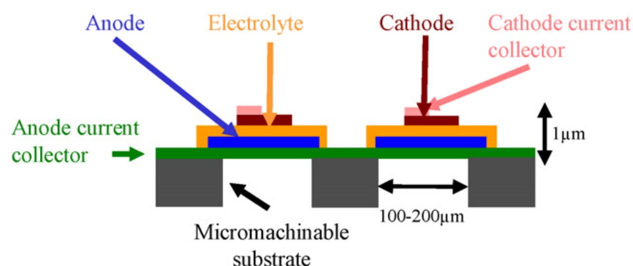

Fig. 1. Schematic view of Foturan®-based μ-SOFC membranes.

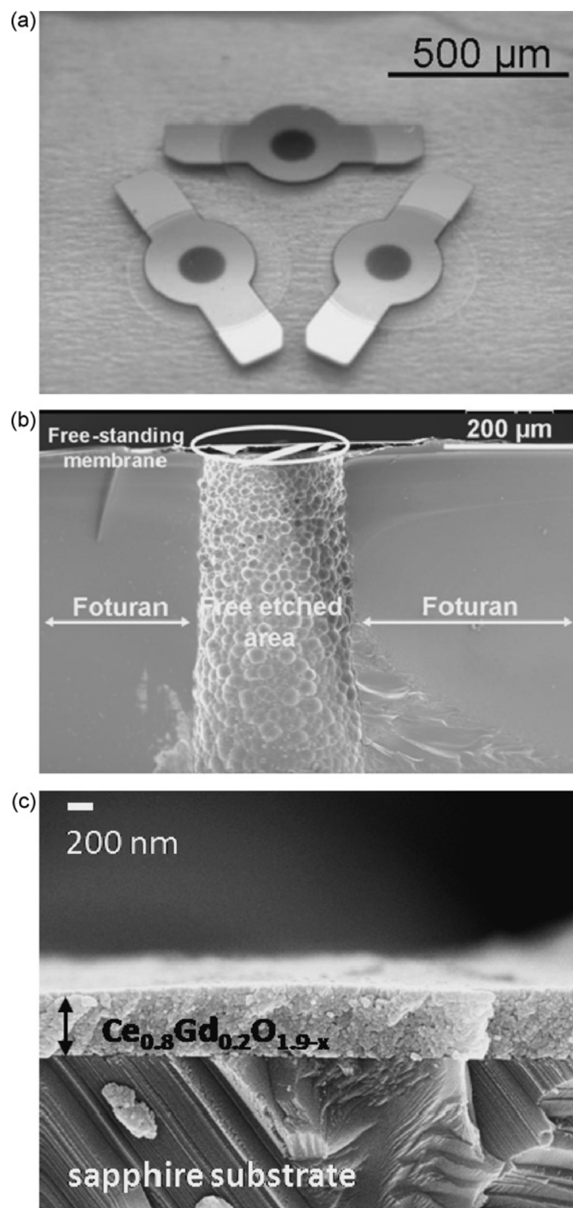

Fig. 2. (a) Top-view light microscopy picture of three individual μ-SOFC membranes on a Foturan® chip with dimension 2.5 cm × 2.0 cm. Membranes are 200 μm wide and less than 1 μm thick composed of anode, electrolyte and cathode as thin films, seen as round films, as well as Pt current collectors. (b) Cross-sectional SEM image of free-standing μ-SOFC membrane integrated on a Foturan® wafer substrate. The area underneath the membrane is free-etched via 10% HF acid, after photolithography and masking. (c) State-of-the-art $Ce_{0.8}Gd_{0.2}O_{1.9-x}$ spray pyrolysis thin film electrolyte for μ-SOFC membranes on substrate. This film is shown after annealing at 1100 °C to full crystallinity.

2. Dry- and wet-chemical etching of ceria-based thin films towards microfabrication

Ceria-based materials are ambitious to microstructure via etching due to their ability to undergo changes in their oxidation state within the redox couple Ce^{4+}-Ce^{3+} with consequent formation or annihilation of oxygen vacancies [15]. It is known that ceria-based films are highly resistant towards most commonly used wet-etching agents, including strong acids and their mixtures, e.g. aqua regia [16]. The reason for this is the poor solubility of the Ce^{4+} ions and the strong tendency to stabilize easily in a complex action such as chloro- or amino-complexes. Contrary to Ce^{3+} which forms soluble compounds in most acidic aqueous solutions, and this ability needs to be taken into account for wet-etching. It was proven by Kossoy that the use of reducing acidic etch solvents, i.e. $HCl + K_4[Fe(Cn)_6]$ or $HNO_3 + FeSO_4{\cdot}7H_2O$ are ideal solutions for structuring through wet-chemistry [16]. Most interestingly reducing acidic etchants do not attack common microfabrication materials such as SiO_2, Si_3N, or metals such as Cu, Ag or Au, and would even allow for distinctive patterning. Dry-etching etches ceria-based materials [17] and conventional Si_3N_4 electrical insulation coatings [18] at almost equal etch-rates around 0.01 $\mu m\,min^{-1}$ and therefore hardly allows one define etch stops (Tables 1 and 2). Among the wet-chemical etchants only HF acid were reported as well as the reducing acidic etchants [19]. Latterly wet-etchant becomes even more relevant in view of the limited structuring of Foturan® glass ceramic wafer substrates to HF acid. However, etch-rates for ceria-based thin films are unpublished and cannot be revealed towards Foturan® glass ceramic wafer substrates to judge on their ability to act as potential etch stops.

Dry-chemical etching is in contrast to wet-chemical etching highly directional through ion bombardment [18]. The consequence is the ability of the thin films to show undercuts towards the substrate. For microfabrication of electroceramic devices this is undesirable since variations in the dimensions of an electroceramic thin film affect the current distributions and ohmic resistances. Pure Ar^+ ion etching through physical destruction of Ce–O bonds were reported, these experiments were initially performed for depth profiling in SIMS and XPS analysis (and not intended for microfabrication) [17]. Reactive ion etching through Ar^+/CF_4 or Ar^+/Cl_2 plasmas were discussed for microfabrication of FRAM (ferroelectric random access memories) [20]. Amongst the dry etchants reactive ion etching is one of the best choices as the etch-rates are higher, around 0.025 $\mu m\,min^{-1}$, and it is less directional compared to pure Ar^+ ion bombardment. In dry-etching techniques the formation of low-volatile Ce chlorides and fluorides through the formation of low volatiles, adds to the pure physical cracking of ceria bonds. Comparison of reactive ion etch-rates for ceria-based films to those of Si-based microfabrication substrates revealed that these are very closely related (Tables 1 and 2).

Etch-rates and etchants reported in literature are summarized for ceria-based materials and can be compared to those of standard microfabrication substrates, i.e. Si, Si_3N_4 or Foturan® glass–ceramic as shown in Tables 1 and 2, respectively.

Considering the variable nature of ceria-based thin film microstructures it remains questionable which role the initial film processing and post-deposition thermal history has on future etch-resistance. Their role as etch stops is therefore hard to predict and needs further attention. It is known from literature that the choice of a thin film deposition method has a high impact on its deposited microstructure and thermal evolution. Two classifications of thin film methods can be grouped together: precipitation-based (i.e. sol–gel, spray pyrolysis or CVD) and vacuum-based (i.e. PVD or PLD) thin film deposition techniques. In both thin film groups, materials can vary from isotropic structures with round nanocrystalline grains or fully amorphous films to anisotropic microstructures,

Table 1
Common etch-rates for dry- and wet-chemical etchants towards ceria-based materials in known literature.

Material	Processing	Etch-rate (μm min^{-1})	Etchant	Dry-chemical etching	Wet-chemical etching	Ref.
$Ce_{0.8}Gd_{0.2}O_{1.9-x}$	Sintered pellet	–	HF		X	[19]
	Spray pyrolysis thin film	0.011	Ar^+	X		[17]
CeO_{2-x}	RF sputtered thin film	0.0002–0.001	$HCl + K_4[Fe(Cn)_6]$		X	[16]
		0.003	$HNO_3 + FeSO_4{\cdot}7H_2O$		X	
		0.01–0.02	$Ar(80) + CF_4(20)$	X		[20]
		0.003–0.025	$Cl/(Ar(80) + CF_4(20))$	X		

Table 2
Common etch-rates for dry- and wet-chemical etchants towards microfabrication substrates in literature.

Material	Processing	Etch-rate (μm min^{-1})	Etchant	Dry-chemical etching	Wet-chemical etching	Ref.
Si	Wafer	0.0005–0.01	KOH		X	[18]
Si_3N_4	LPCVD	0.025	$O_2(4) + CF_4(96)$	X		
Foturan®	Glass–ceramic wafer	10–20	10% $HF:H_2O$		X	[7,10]

i.e. biphasic amorphous–crystalline phases, crystal orientations or columnar grains [21]. Full crystallization of thin films to exclude residual amorphous phase is, in many cases, impossible with respect to temperature as the μ-SOFC substrates cannot exceed 800 °C. With higher temperatures Foturan® glass–ceramic wafers melt [10] and Si-based wafers start to oxidize [18].

Precipitation- and vacuum-processed thin films differ strongly in their chemical valence and even composition after film deposition: vacuum-based films show a major tendency to crystallize in columns and pronounced anisotropies in the thin film microstructures results. In general, pronounced orientation of a material can lead to severe anisotropy towards a wet-etchant such as KOH etching of oriented Si-wafers [22], and etching at non-perpendicular angles or undercuts results. Moreover, the reducing conditions of vacuum processing can lead to pronounced reduction of materials, e.g. ceria-based. Contrary, precipitation-based films always contain salt rests such as chlorine, fluorine, ammonia and different amounts of hydroxyl or carbon groups from the solvents due to their preparation based on precursors. It was shown in literature that these residues, i.e. Cl or C, can remain in the material up to high temperatures and incorporate ceria resulting in low packaging densities [23–25]. In addition, these chemical residues affect the crystallization and grain growth kinetics through thermal post-annealing of the material [26].

Due to the fact that wet-chemical etching is based on the formation of volatile compounds with Ce ions results in homogeneous and well controllable etching, it is most likely that chemical residuals from precursor rests in precipitation-based films may facilitate the etching. In this respects strong differences between the etch-resistance of precipitation- and vacuum-based thin films are to be assumed.

Nevertheless, it can be summarized that especially the role of a thin film microstructure on the etch ability and resistance towards an etch-resistance is completely unknown, but is of high relevance for microfabrication of μ-SOFC devices.

In this paper we study the impact of the wet-chemical etchant HF acid on $Ce_{0.8}Gd_{0.2}O_{1.9-x}$ electrolyte thin films fabricated via wet-chemical precipitation method, spray pyrolysis. Latterly a deposition method was chosen to deposit $Ce_{0.8}Gd_{0.2}O_{1.9-x}$ thin films since it is a relatively low-cost and precipitation-based method for μ-SOFC fabrication. Film properties, i.e. crystallization, grain growth, electric and thermodynamic stability were well characterized for this material in previous studies [13,14,17,26–28]. Etch-resistance of these films towards 10% $HF:H_2O$ was investigated with respect to exposure time and ambient microstructure ranging from fully crystalline to biphasic amorphous–crystalline. Etch-rates will be compared against other etchants and discussed for state-of-the-art microfabrication substrates. Specific guidance for future μ-SOFC processing based on precipitation-based thin films and wet-etching of Foturan® wafer substrates will be given.

3. Experimental

3.1. Thin film preparation

Gadolinia-doped ceria (CGO = $Ce_{0.8}Gd_{0.2}O_{1.9-x}$) spray pyrolysis precursor solutions were made from 0.02 mol l^{-1} gadolinium chloride (Alfa Aesar, 99.9% purity) and 0.08 mol l^{-1} cerium nitrate (Alfa Aesar, 99% purity) dissolved in 10:90 vol.% water and tetraethyleng-lykol (Aldrich, >99% purity). These precursor solutions were fed to a spray gun (Compact 2000KM, Bölhoff Verfahrenstechnik, Germany) with a liquid flow rate of 5 ml h^{-1} and atomized with 1 bar air pressure. The droplets produced in this manner were sprayed on a heated sapphire single crystal substrate (Stettler, Switzerland) at 390 ± 5 °C for 1 h. The working distance between the spray nozzle and the hot plate was kept at 45 cm during all experiments. The spray pyrolysis process is described in further detail elsewhere [29–32]. After spray pyrolysis the films are amorphous and can be converted to biphasic amorphous–nanocrystalline or totally nanocrystalline films by post-annealing at higher temperatures than the spray pyrolysis deposition temperature [27,28]. For this investigation thin films were annealed with 3 °C min^{-1} heating and cooling rate to either 600 or 1000 °C with an isothermal hold of 10 min in air at the maximum temperature. By this annealing step crystallization of the originally amorphous films is induced.

3.2. Chemistry of the thin films

The chemical composition of the as-deposited films were determined by energy dispersive X-ray spectroscopy (EDX, Leo 1530, Germany) using the cerium and gadolinium L-lines at 20 kV. For quantitative EDX analysis, the Proza correction method was chosen.

3.3. Crystallization and grain growth of the thin films

Crystallization and average grain size was determined by X-ray diffraction (XRD, Bruker AXS D8 Advance). Samples were annealed in situ (Anton Paar HTK 1200), where the change in line width of the Bragg peaks provided information on the average grain size. Diffracted X-rays from the sample were detected by a position sensitive detector (Braun PSD ASA-S). The XRD setup entailed a copper radiation source (λ = 0.15404 nm) operated at 40 kV and 40 mA with a Kα_1-Ge monochromator (Bruker AXS). The average

grain size was determined from the full width at half maximum (*FWHM*) and using Fourier analysis of the XRD peaks, refined by a split Pearson 7 function (Software EVA 6.0). The *FWHM* results from instrumental broadening and thin film microstructure. The instrumental peak broadening of the diffractometer was determined by measuring a commercially available microcrystalline and stress-free macrocrystalline gadolinia-doped ceria powder of large particles. The instrumental broadening can be eliminated from the *FWHM* using the Warren and Biscoe equation [33]. Average grain size was calculated according to the Scherrer equation [34,35].

Crystallization of the amorphous spray pyrolysis thin films during subsequent annealing were measured in calibrated differential scanning calorimetry (DSC/TG, Netzsch STA 449C) experiments. These measurements enable the degree of crystallinity from the exothermic heat loss reading and the amount of amorphous versus crystalline phase to be determined. In order to quantify the DSC results, the instrument was calibrated with calibration standards (Netzsch 6.223.5-91.2) of known melting points and heat losses. Material from the as-deposited amorphous thin films were scratched off from the sapphire substrates and 50 ± 1 mg of powder was enclosed in a closed Pt pan and measured against an empty closed Pt pan as reference. Non-isothermal DSC readings were recorded from room temperature to 1100 °C at 6 °C min^{-1} under static air atmosphere. Fully crystallized $Ce_{0.8}Gd_{0.2}O_{1.9-x}$ spray pyrolysis powder was measured under the same experimental conditions in order to correct the quantitative DSC analysis. The result of this experiment was recorded and subtracted from the other measured results of partially crystallized materials.

3.4. HF etching of the thin film microstructures

The films were etched in 10% HF:H_2O acid at room temperature under constant stirring after annealing the $Ce_{0.8}Gd_{0.2}O_{1.9-x}$ thin films at 600 or 1000 °C.

The microstructures of the thin films were characterized using scanning electron microscopy (SEM, Leo 1530, Germany). The top layer of a thin film was sputtered (Bal-Tec, SCD 050, Sputter Coater) with Pt in order to avoid charging and to allow imaging at higher resolutions. Average grain sizes of the thin films in respect to annealing temperature and impact of HF acid during etching were evaluated by linear intercept length analysis with program LINCE 2.31D from SEM micrographs. Conversion rate of intercept length to grain size was obtained by multiplying the grain size conversion factor of 1.56. The etch-rate of HF acid on the thin films was quantified by change in image contrast between crystalline grains and substrate by Image J 1.33u.

4. Results and discussions

4.1. Thermal annealing of precipitation-based $Ce_{0.8}Gd_{0.2}O_{1.9-x}$ spray pyrolysis thin films

The typical microstructure of a post-annealed $Ce_{0.8}Gd_{0.2}O_{1.9-x}$ spray pyrolysis thin film is displayed in the SEM cross-section of Fig. 2(c). The gadolinia-doped ceria films selected for this etch-resistance study were always dense and had a crack-free microstructure with an overall film thickness of 100 ± 15 nm after film deposition. It is also shown in the SEM cross-sectional microstructure that the grains of the films were isotropically distributed over the film. General details on these thin film microstructures can be found elsewhere [27,28].

The evaluation of microstructure of as-deposited $Ce_{0.8}Gd_{0.2}O_{1.9-x}$ spray pyrolysis thin films with temperature were studied via X-ray diffraction is shown in Fig. 3. As-deposited films show no clear Bragg diffractions only broad halos around

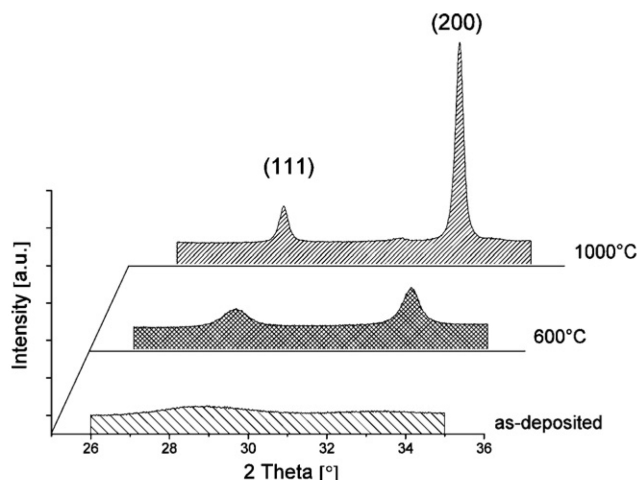

Fig. 3. XRD analysis of $Ce_{0.8}Gd_{0.2}O_{1.9-x}$ spray pyrolysis thin films with respect to temperature.

the diffraction angles. The precipitation-based films are X-ray amorphous directly after deposition. Sharp XRD peaks develop with higher temperature increments and crystallization, in accordance with the cubic fluorite crystal lattice of the gadolinia-doped ceria [36]. XRD analysis is in agreement with EDX confirming the presence of 22 ± 2 cat% gadolinia in the ceria lattice [17,27].

The most intense XRD peak is always the (2 0 0) peak relative to the (1 1 1) peak. All annealed films within this study show isotropically distributed grains over the film with a (2 0 0) orientation perpendicular to the substrate. This is in agreement with previous

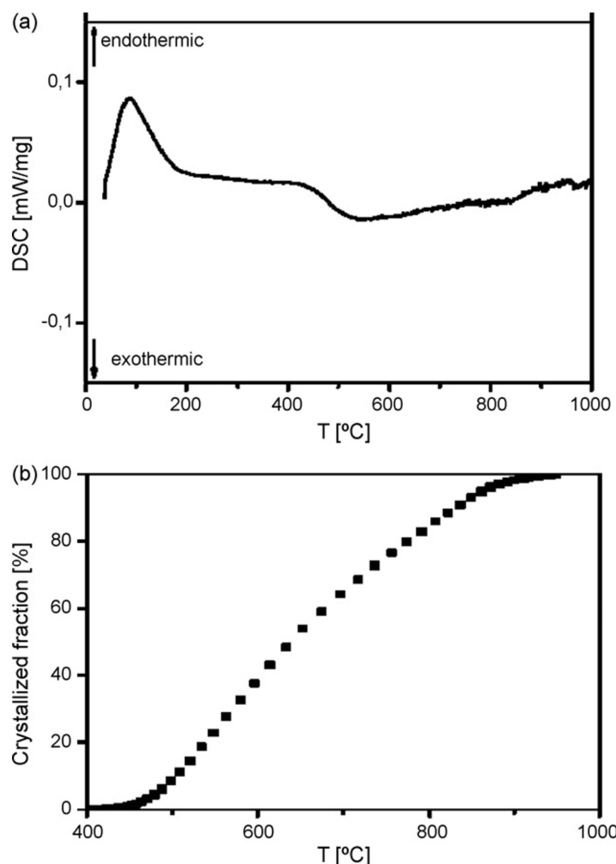

Fig. 4. (a) Non-isothermal DSC signal of $Ce_{0.8}Gd_{0.2}O_{1.9-x}$ spray pyrolysis thin films for 6 °C min^{-1} heating rate in static air atmosphere. (b) Calculated fraction of crystallized material from the exothermic crystallization peak signal of DSC analysis.

studies on gadolinia-doped ceria films deposited by precipitation as spray pyrolysis [27], sol–gel [37], or CVD [38].

Non-isothermal crystallization, as well as general heat fluxes, of the $Ce_{0.8}Gd_{0.2}O_{1.9-x}$ spray pyrolysis thin films were recorded via DSC for ±6 K min^{-1} (Fig. 4(a)). At low temperature an endothermic reaction is observed with a peak maxima at 120 °C, which, corresponds to the desorption of residual water. Between 400 and 1000 °C there is a broad exotherm coincident resulting from the heat release during crystallization of the sample. In general, such an exothermic DSC heat release reflects the transformation of an amorphous to a crystalline phase and is proportional to the crystallization enthalpy of the material [39–41]. Kinetic measures such as crystallization enthalpy, as well as full Johnson–Mehl–Avrami (JMA) analysis for nucleation and crystallization characteristics can be reasonably analyzed for precipitation-based metal oxide thin films, in a similar manner to state-of-the-art studies in glass–ceramics via classic DSC experiments [26]. In Fig. 4(b), the calculated crystallized fraction versus temperature plot is displayed for the DSC exotherm. This reveals a typical sigmoidal JMA curve shape, as shown in previous studies for precipitation-based metal oxide thin films [26] and conventional glass–ceramics [41–44]. The nucleation phase indicated by the non-linear correlation between crystallized fraction and temperature, around 400–460 °C, proceeds within a very short temperature frame of $\Delta T = 30$ °C. Nucleation starts just briefly above the deposition temperature, around 390 °C, a temperature increase of only 10 °C is required to initiate crystallization of these films. This demonstrates that the amorphous material contains enough nuclei for crystallization, which is typical for the kind of metal oxides prepared from organo-metallic complexes by precipitation [26]. The crystalliza-

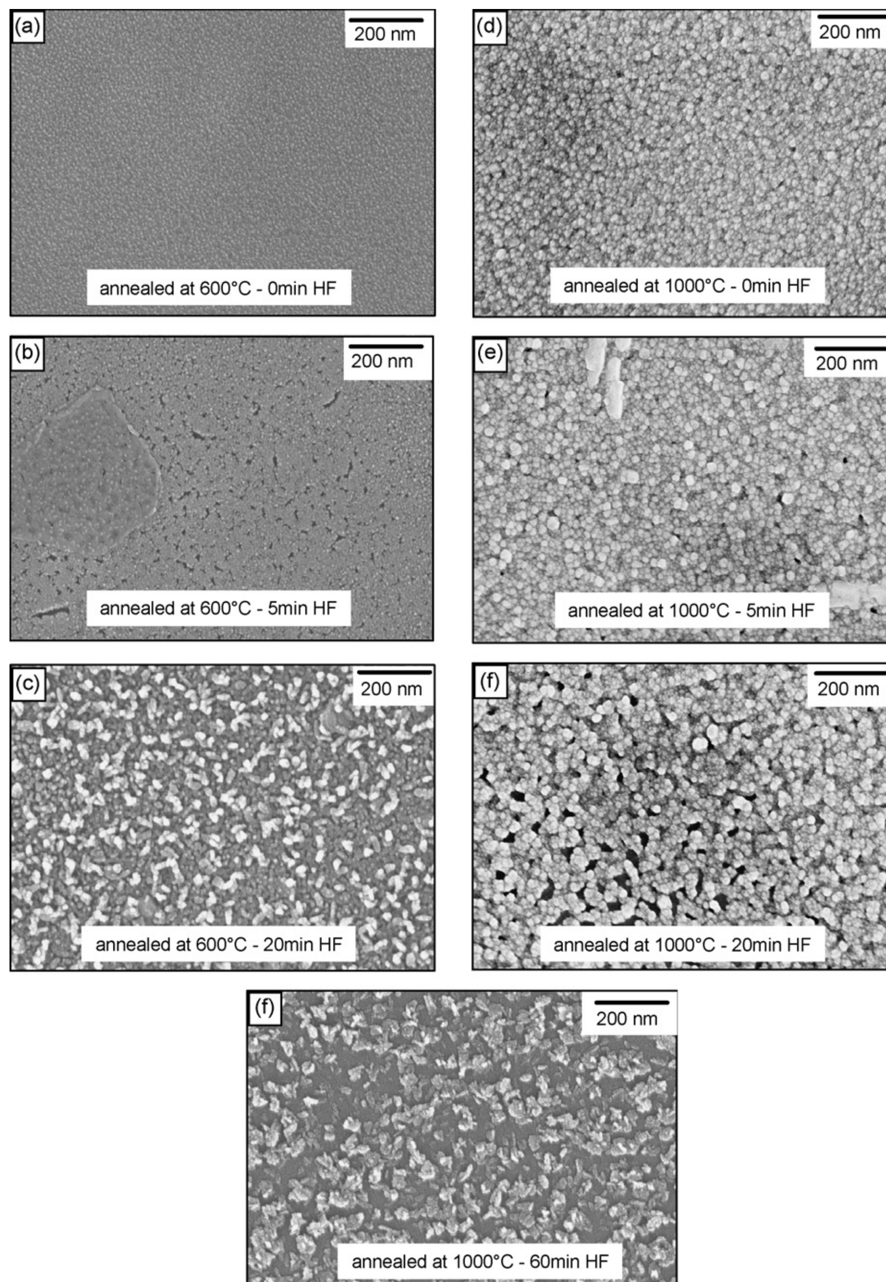

Fig. 5. SEM top-view micrographs of 100 nm thick $Ce_{0.8}Gd_{0.2}O_{1.9-x}$ spray pyrolysis thin films on sapphire substrates with respect to annealing temperature and HF acid exposure time. The impact of HF on microstructures is shown for thin films annealed at 600 °C: (a) 0 min, (b) 5 min and (c) 20 min HF exposure time, and for thin films annealed at 1000 °C: (d) 0 min, (e) 5 min, (f) 20 min and (g) 60 min HF exposure time.

tion of the material proceeds over a wide temperature range of $\Delta T = 600\,^{\circ}\mathrm{C}$, indicated by the linear behavior of crystallized fraction versus temperature. Full crystallinity is reached around 950 °C with a characteristic Kissinger activation energy of crystallization [45] of 96.5 J g^{-1} for the $Ce_{0.8}Gd_{0.2}O_{1.9-x}$ films. Details on evaluation of Kissinger activation energy for metal oxide thin films are given elsewhere [26].

It can be concluded from this DSC-based crystallization study that the XRD-sample annealed at 600 °C is biphasic amorphous–crystalline with 62% amorphous residual phases, whereas the film annealed at 1000 °C is fully crystalline as crystallization has clearly been accomplished. The annealing temperature of the biphasic film represents the state-of-the-art maximum temperature of Foturan®-based μ-SOFCs during processing [5]. Heating above 800 °C would harm the substrate in fabrication. Both $Ce_{0.8}Gd_{0.2}O_{1.9-x}$ thin films were exposed to HF acid as they differ strongly in their degree of crystallinity at equal (2 0 0) grain orientation and film thickness.

4.2. Etch-resistance towards HF acid of precipitation-based $Ce_{0.8}Gd_{0.2}O_{1.9-x}$ spray pyrolysis thin films

The influence of 10% HF:H_2O acid on $Ce_{0.8}Gd_{0.2}O_{1.9-x}$ spray pyrolysis thin film microstructures were studied with respect to exposure time to the acid, and are shown in Fig. 5. The 10% concentration of the HF is chosen in accordance with the fabrication guidelines for structuring of Foturan® glass–ceramic wafers given by the supplier. In Fig. 5(a) and (d), SEM micrographs of the unexposed biphasic amorphous–crystalline and fully nanocrystalline thin films annealed at 600 and 1000 °C are displayed, respectively. In addition, these samples differ in their average grain size, i.e. more than doubled the 40 nm for the samples annealed at higher temperature. The overall film thickness evaluated via SEM was approximately 100 ± 15 nm, and used for all films in this study.

Irrespective of the degree of crystallinity and average grain size, HF acid attack caused severe damage to the films after 5 min. A closer inspection at the etched film surface, showed that the etchant removes the top layer of the film first, as only residual patches of the top layers remained (Fig. 5(b) and (e)). Increasing the etch time to 60 min lead to attacking and etching of grain boundaries (Fig. 5(c), (f) and (g)).

In general, the biphasic amorphous–crystalline films were attacked more (after shorter times) by HF acid than the fully crystalline ones. This is especially visible in the comparison of the 20 min exposed microstructures to HF acid. A completely disconnected biphasic film remains with visible parts of the substrate and a connected microstructure with large pores and partially etched grain boundaries were visible for the fully crystalline one (Fig. 5(c) and (f)). Complete disconnection remaining parts of the substrate were only visible for the fully crystalline film in the case of the 60 min etched film.

Etching rates of 2.54 ± 0.1 and 0.62 ± 0.03 area% min^{-1} for 10% HF:H_2O in $Ce_{0.8}Gd_{0.2}O_{1.9-x}$ films were determined from linear fits of the biphasic and fully crystalline films, respectively. It can be concluded that increasing the crystallinity enhances the resistance of $Ce_{0.8}Gd_{0.2}O_{1.9-x}$ thin films against exposure to HF acid (Fig. 6).

One can also assess the relative etch-rates through the film thickness from the SEM micrographs, i.e. etching through the substrate (Fig. 5(c), (f) and (g)). In case of the biphasic and fully crystalline $Ce_{0.8}Gd_{0.2}O_{1.9-x}$ thin film 10% HF:H_2O etch-rates are 0.005 ± 0.001 to 0.002 ± 0.001 μm min^{-1}, respectively. Latterly etch-rate errors are higher relative to the area etch-rate errors since the exact time for etching completely through the film to the substrate is less precisely given.

Etch studies on fully amorphous $Ce_{0.8}Gd_{0.2}O_{1.9-x}$ thin films revealed that films are completely etched in less than 1 min attack

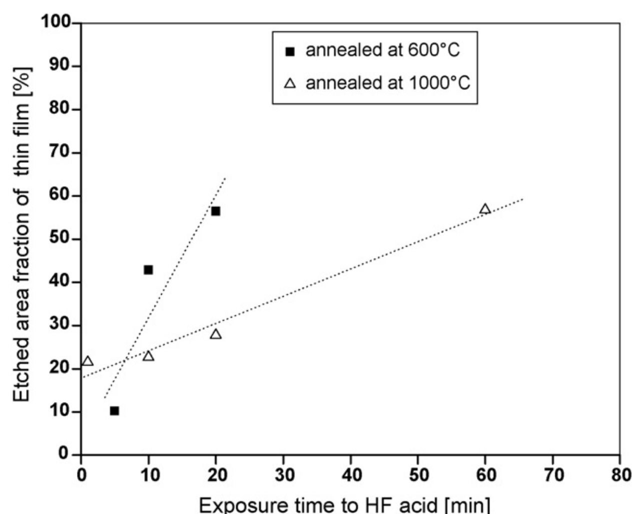

Fig. 6. Etched away area fraction determined from SEM top-views of 100 nm thick $Ce_{0.8}Gd_{0.2}O_{1.9-x}$ spray pyrolysis thin films on sapphire substrates with respect to their exposure time in 10% HF acid concentrate and previous annealing temperature.

to 10% HF:H_2O. No etch-rate was determined since the time span until full disappearance was too short to establish precise data points for amorphous thin films.

Comparison of known literature reveals that the etch-rates of the spray pyrolysis $Ce_{0.8}Gd_{0.2}O_{1.9-x}$ films for etching in 10% HF:H_2O are close to those for dry- or other reducing acid wet-etchants (Table 3). Varying microstructures in their degree of crystallinity had a strong effect on the etch-rate. Quantitative changes were as large as etch-rate changes due to usage of different etchants for equal ceria-based film microstructures, i.e. changing the reaction gas in a dry-etching process or switching between totally different wet-chemicals (Tables 1 and 3). Increase of amorphous phase and the consequential lowering of the packaging density of the film material increased its etch-rate.

All etch-rates of $Ce_{0.8}Gd_{0.2}O_{1.9-x}$ thin films are extremely close to conventional Si-wafers or their electric insulation coatings, i.e. Si_3N_4. The largest discrepancy in etch-rate was observed between the $Ce_{0.8}Gd_{0.2}O_{1.9-x}$ films and the Foturan® glass–ceramic wafers (Table 3).

4.3. Guidance for the Foturan® -based μ-SOFC processing with precipitation-based electrolyte thin films: thermal annealing and etching

The free-etching of μ-SOFC substrates has to be well controlled under laboratory conditions, since over-etching of the membranes for too long time spans results in their cracking and damage. As a consequence the etch-rate of the wafer substrate has to be much higher than the one of the $Ce_{0.8}Gd_{0.2}O_{1.9-x}$ thin film on the substrate. According to known literature etch-rates between 10 and 20 μm min^{-1} towards 10% HF:H_2O acid were reported for the crystalline phase of the Foturan® glass–ceramic [7,10]. These etch-rates were triple in magnitude compared to that of $Ce_{0.8}Gd_{0.2}O_{1.9-x}$ thin films measured (Table 3). Even though the difference in etch-rates between the μ-SOFC electrolyte thin film and the Foturan® wafer substrate is large this does not signify the thin film as a good etch stop. According to literature, Foturan® etching proceeds over the grain boundaries whereby its grains disconnect and fall out [8–10]. Since its grains are in tenths of microns in size within 1 min already one grain layer is etched according to its etch-rate. This signifies that the engineer has to know by the minute precisely when the Foturan® is etched through otherwise HF acid will severely damages the $Ce_{0.8}Gd_{0.2}O_{1.9-x}$ thin film microstructures by creeping in

Table 3
Comparison of etch-rates for $Ce_{0.8}Gd_{0.2}O_{1.9-x}$ electrolyte thin films made by the precipitation-based spray pyrolysis method towards μ-solid oxide fuel cell relevant substrates towards HF acid.

Material	Etch-rate ($\mu m\, min^{-1}$)	Microstructure	$HF:H_2O$ concentration (%)	Ref.
$Ce_{0.8}Gd_{0.2}O_{1.9-x}$ spray pyrolysis thin films	0.002	Fully crystalline	10	This study
	0.005	Biphasic: amorphous–crystalline (38% crystalline phase)		
Foturan® glass–ceramic wafer	10	Crystalline, ceramic phase		[10]
	20			[7]
Si_3N_4 LPCVD thin film (common electric insulation coating on Si-wafer)	0.02	Crystalline	40	[18]

its grain boundaries and dissolving potential amorphous residual phases. Moreover, the impact of HF acid on the electric properties of μ-SOFC thin films for low exposure times is still to be investigated and may affect, apart from mechanical stability of the fuel cell membrane, also its power performance.

Etching the Foturan-based μ-SOFCs with a lower concentrated HF acid solution, i.e. 1% $HF:H_2O$ may be a suitable solution to gain a better control of the free-etching process once it is close to the membrane. In a first step most of the substrate could be etched with 10% $HF:H_2O$ until the last 100 μm of substrate underneath the thin film remains to benefit from the high etch-rate. In a second step, the membrane could be free-etched by the use of a lower concentrated HF acid bath, i.e. 1% $HF:H_2O$ to reduce the damage of HF acid on the film microstructure during free-etching and membrane formation.

5. Conclusions

In this paper the impact of 10% $HF:H_2O$ as a typical wet-chemical etchant in μ-SOFC fabrication on $Ce_{0.8}Gd_{0.2}O_{1.9-x}$ thin film made by spray pyrolysis was studied. The progress in film microstructures impact of the etchant, as well as corresponding etch-rates were determined.

Known literature comparison clearly revealed that there is a strong dependency of thin film microstructure (i.e. degree of crystallinity) on the etch-rate of $Ce_{0.8}Gd_{0.2}O_{1.9-x}$ thin films. The impact of microstructure on the etch-rate is even as large as changing the etchant in a dry- or wet-chemical etching procedure for an equal film microstructure. In general, the etch-rates of $Ce_{0.8}Gd_{0.2}O_{1.9-x}$ thin films, Si or Si_3N_4 towards HF acid and other dry- and wet-chemical etchants are extremely close, thus, challenging for Si-based microfabricated devices. Most interestingly a strong difference exists in the case of Foturan®glass ceramic wafers.

Therefore, we would like to give the following general guidelines concerning free-etching and thermal annealing steps for Foturan®-based μ-SOFC fabrication:

1. *Isothermal annealing steps during fabrication*. Crystallization of precipitation-based thin films to fully crystalline films increases their etch-resistance towards wet-chemical HF acid severely. It was shown in previous studies that crystallization could be accomplished for precipitation-based thin films for isothermal annealing of more than 10 h at 600–800 °C [26,27], which would also be a harmless annealing temperature for Foturan® (and also Si) wafers. The damage of HF acid on the $Ce_{0.8}Gd_{0.2}O_{1.9-x}$ thin film microstructures can be kept to a minimum, as it can only attack grain boundaries, but not larger residual amorpous phases.
2. *Free-etching of the $Ce_{0.8}Gd_{0.2}O_{1.9-x}$ thin film*. Keeping the actual time of fuel cell membrane free-etching as short as possible, over-etching can be avoided. The $Ce_{0.8}Gd_{0.2}O_{1.9-x}$ thin film may be a good etch stop in terms of the etch-rate, but the thin films get damaged early for short time spans by the HF acid in the grain boundaries. Since the Foturan® etch-rates are a factor of 1000 or *larger*, and its etching progresses fast, it is a major challenge to avoid that the thin film is exposed for a time span longer than 1 min. In case of longer etching exposure of the $Ce_{0.8}Gd_{0.2}O_{1.9-x}$ thin film, we can confirm severe effects on the film microstructures, but the overall impact on its power performance or mechanical stability is unclear. Lowering the concentration of the HF acid to a solution of 1% $HF:H_2O$ may result in a better control of the thin film free-etching process, and less damage to the thin film microstructure.

References

[1] A. Bieberle-Hütter, D. Beckel, U.P. Muecke, J.L.M. Rupp, A. Infortuna, L.J. Gauckler, MST News, VDI 4 (2005) 12–15.
[2] A. Bieberle-Hutter, D. Beckel, A. Infortuna, U.P. Muecke, J.L.M. Rupp, L.J. Gauckler, S. Rey-Mermet, P. Muralt, N.R. Bieri, N. Hotz, M.J. Stutz, D. Poulikakos, P. Heeb, P. Muller, A. Bernard, R. Gmur, T. Hocker, J. Power Sources 177 (1) (2008) 123–130.
[3] A. Evans, A. Bieberle-Hütter, H. Galinski, J.L.M. Rupp, T. Ryll, S. Barbara, R. Tölke, L.J. Gauckler, Monatsheft für Chemie 140 (9) (2009) 975–983.
[4] H. Huang, M. Nakamura, P.C. Su, R. Fasching, Y. Saito, F.B. Prinz, J. Electrochem. Soc. 154 (1) (2007) B20–B24.
[5] U.P. Muecke, D. Beckel, A. Bernard, A. Bieberle-Hütter, S. Graf, A. Infortuna, J.L.M. Rupp, J. Schneider, P. Müller, J. Gauckler, Adv. Funct. Mater. 18 (20) (2008) 3158.
[6] J.H. Shim, C.-C. Chao, H. Huang, F.B. Prinz, Chem. Mater. 19 (2007) 3850.
[7] Y.-R. Cho, J.-Y. Oh, H.-S. Kim, H.-S. Jeong, Mater. Sci. Eng. B 64 (2) (1999) 79–83.
[8] D. Hülsenberg, R. Bruntsch, J. Non-Cryst. Solids 129 (1–3) (1991) 199–205.
[9] D. Hülsenberg, Microelectron. J. 28 (4) (1997) 419–432.
[10] T.R. Dietrich, W. Ehrfeld, M. Lacher, M. Krämer, B. Speit, Microelectron. Eng. 30 (1–4) (1996) 497–504.
[11] L.J. Gauckler, D. Beckel, U.P. Mücke, P. Müller, J.L.M. Rupp, Dünnfilme und damit hergestelltes Verbundelement, Europäisches Patent, 2005, No. 1683/05 (applied for).
[12] L.J. Gauckler, D. Beckel, U.P. Mücke, P. Müller, J.L.M. Rupp, Verbundelement, Europäisches Patent, 2005, No. 1682/05 (applied for).
[13] J.L.M. Rupp, A. Infortuna, L.J. Gauckler, J. Am. Ceram. Soc. 90 (6) (2007) 1792–1797.
[14] J.L.M. Rupp, L.J. Gauckler, Solid State Ionics 177 (2006) 2513.
[15] M. Mogensen, N.M. Sammes, G.A. Tompsett, Solid State Ionics 129 (1–4) (2000) 63–94.
[16] A. Kossoy, M. Greenberg, K. Gartsman, I. Lubomirsky, J. Electrochem. Soc. 152 (2) (2005) C65–C66.
[17] J.L.M. Rupp, T. Drobek, A. Rossi, L.J. Gauckler, Chem. Mater. 19 (5) (2007) 1134–1142.
[18] M.J. Madou, Fundamentals of Microfabrication, The Science of Miniaturization, Second edition, CRC Press, 2002.
[19] J.M. Bae, B.C.H. Steele, Solid State Ionics 106 (3–4) (1998) 247–253.
[20] D.P. Kim, Y.S. Chang, C.I. Kim, J. Vac. Sci. Technol. A 22 (2) (2004) 441–1441.
[21] D. Beckel, A. Bieberle-Hutter, A. Harvey, A. Infortuna, U.P. Muecke, M. Prestat, J.L.M. Rupp, L.J. Gauckler, J. Power Sources 173 (1) (2007) 325.
[22] M.J. Madou, Anisotropic Wet Etching, 2002, p. 190.
[23] L. Kepinski, J. Okal, J. Catal. 192 (1) (2000) 48–53.
[24] C. Force, J.P. Belzunegui, J. Sanz, A. Martinez-Arias, J. Soria, J. Catal. 197 (1) (2001) 192–199.
[25] N.J. Clark, I.J. McColm, J. Inorg. Nucl. Chem. 34 (1972) 117–123.
[26] J.L.M. Rupp, B. Scherrer, A. Harvey, L.J. Gauckler, Adv. Funct. Mater. 19 (1) (2009) 1–10.
[27] J.L.M. Rupp, A. Infortuna, L.J. Gauckler, Acta Mater. 54 (7) (2006) 1721–1730.
[28] J.L.M. Rupp, C. Solenthaler, P. Gasser, U.P. Muecke, L.J. Gauckler, Acta Mater. 55 (10) (2007) 3505–3512.
[29] P.S. Patil, Mater. Chem. Phys. 59 (3) (1999) 185–198.
[30] D. Perednis, L.J. Gauckler, Solid State Ionics 166 (3–4) (2004) 229–239.
[31] D. Perednis, O. Wilhelm, S.E. Pratsinis, L.J. Gauckler, Thin Solid Films 474 (1–2) (2005) 84–95.
[32] O. Wilhelm, S.E. Pratsinis, D. Perednis, L.J. Gauckler, Thin Solid Films 479 (1–2) (2005) 121–129.
[33] C.N.J. Wagner, E.N. Aqua, J. Less Common Met. 8 (1) (1965) 51–62.

[34] P. Scherrer, Bestimmung der Grösse und der inneren Struktur von Kolloidteilchen mittels Röntgenstrahlen, vol. 1, Nachrichten von der Königlichen Gesellschaft der Wissenschaft zu Göttingen: Mathematisch-physikalische Klasse, 1918, pp. 98–100.
[35] A.J.C. Wilson, X-ray Optics, 1949, p. 5.
[36] T.S. Zhang, J. Ma, L.B. Kong, P. Hing, Y.J. Leng, S.H. Chan, J.A. Kilner, J. Power Sources 124 (1) (2003) 26–33.
[37] T. Suzuki, I. Kosacki, H.U. Anderson, Solid State Ionics 151 (1–4) (2002) 111–121.
[38] H.Z. Song, H.B. Wang, S.W. Zha, D.K. Peng, G.Y. Meng, Solid State Ionics 156 (3) (2003) 249–254.
[39] K. Lu, Mater. Sci. Eng. R16 (1996) 161–221.
[40] H.V. Atkinson, Acta Metall. 36 (3) (1988) 469–491.
[41] K.A. Jackson, Kinetic Processes: Chapter 15 Nucleation, Wiley-VCH Verlag Gmbh & Co., KGaA Weinheim, 2004.
[42] M. Avrami, Granulation, J. Chem. Phys. 9 (2) (1941) 177–184.
[43] M. Avrami, J. Chem. Phys. 7 (12) (1939) 1103–1112.
[44] G. Ruitenberg, E. Woldt, A.K. Petford-Long, Thermochim. Acta 378 (1–2) (2001) 97–105.
[45] H.E. Kissinger, J. Res. NBS (1956) 157.